Dynamic Improvement of Series–Series Compensated Wireless Power Transfer Systems Using Discrete Sliding Mode Control

Yun Yang, *Student Member, IEEE*, Wenxing Zhong, *Member, IEEE*, Sitthisak Kiratipongvoot, Siew-Chong Tan, *Senior Member, IEEE*, and Shu Yuen Ron Hui, *Fellow, IEEE*

***Abstract*—This paper presents a discrete sliding mode control (DSMC) scheme for a series–series compensated wireless power transfer (WPT) system to achieve fast maximum energy efficiency (MEE) tracking and output voltage regulation. The power transmitter of the adopted WPT system comprises a dc/ac converter, which incorporates the hill-climbing-search-based phase angle control in achieving minimum input current injection from its dc source, thereby attaining minimum input power operation. The power receiver comprises a buck–boost converter that emulates an optimal load value, following the MEE point determined by the DSMC scheme. With this WPT system, no direct communication means is required between the transmitter and the receiver. Therefore, the implementation cost of this system is potentially lower and annoying communication delays, which deteriorate control performance, are absent. Both the simulation and experiment results show that this WPT system displays better dynamic regulation of the output voltage during MEE tracking when it is controlled by DSMC, as compared to that controlled by the conventional discrete proportional-integral (PI) control. Such an improvement prevents the load from sustaining undesirable overshoot/undershoot during transient states.**

***Index Terms*—Discrete sliding mode control (DSMC), dynamic performance, hill-climbing-search-based phase angle control, maximum energy efficiency (MEE), series–series compensated wireless power transfer (WPT) system.**

I. Introduction

EVER since the patent of wireless power transfer (WPT) based on magnetic resonance and near-field coupling of two-loop resonators was reported by Tesla in 1914 [1], the WPT technique has been widely applied in medical implants [2]–[4], induction heaters [5], electric vehicles [6]–[8], and wireless charging platforms for portable equipment such as cellphones [9]–[14]. Particularly over the last decade, with the emergence of diverse mobile terminals, the "Qi" standard is established by the Wireless Power Consortium (covering more than 210 companies worldwide in more than 16 countries) [15] for more than 600 products [16]. Meanwhile, research activities of WPT systems have intensified in aspects relating to magnetic coupling [17]–[21], circuit compensation [7], [8], [21], [22], modeling and control [23]–[28], and basic operating principles, such as maximum power transfer (MPT) principle and maximum energy efficiency (MEE) principle [21], [28], [29]. In the review given in [29], it has been clarified that the MPT principle and the MEE principle should be respectively used for specific applications. WPT systems operating under the MPT principle will never achieve a system's energy efficiency of higher than 50%. However, its achievable transmission distance is longer than that of the same WPT systems operating under the MEE principle. Nevertheless, WPT systems operating under the MEE principle can easily achieve an energy efficiency of higher than 50%.

In this paper, the MEE principle is adopted for the investigated WPT system with series–series compensation. The decision on using this compensation instead of series–parallel compensation, parallel–parallel compensation, or parallel–series compensation is because the series–series compensation is independent of load or mutual inductance [25]. However, series–series compensated WPT systems that operate under the MEE principle suffers from power-efficiency variation when the coupling coefficient, quality factor, and load conditions change [26]–[28]. A mismatch of these parameters between the designed system and the actual system will result in a reduction of system's energy efficiency. To resolve this issue, dynamic MEE tracking schemes are adopted in WPT systems operating in MEE, as reported in [26]–[28]. In [28], the automatic MEE tracking scheme involves a switched-mode converter at the receiver side to emulate the optimal load of minimizing the input power at the transmitter. This scheme is free of communication between the transmitter and the receiver. While it performs accurate tracking

Manuscript received June 9, 2017; revised July 27, 2017; accepted August 26, 2017. Date of publication August 29, 2017; date of current version March 5, 2018. This work was supported by Hong Kong Research Grant Council under theme-based Research Project T23-701/14-N. Recommended for publication by Associate Editor D. Qiu. *(Corresponding author: Yun Yang.)*

Y. Yang, S. Kiratipongvoot, and S. C. Tan are with the Department of Electrical and Electronic Engineering, The University of Hong Kong, Hong Kong, China (e-mail: cacalotoyangyun@gmail.com; ksitthis@eee.hku.hk; sctan@eee.hku.hk).

W. Zhong is with the Department of Electrical Engineering, Zhejiang University, Hangzhou 310058, China (e-mail: wxzhong@zju.edu.cn).

S. Y. R. Hui is with the Department of Electrical and Electronic Engineering, The University of Hong Kong, Hong Kong, China, and also with the Department of Electrical and Electronic Engineering, Imperial College London, London SW7 2AZ, U.K. (e-mail: ronhui@eee.hku.hk).

Color versions of one or more of the figures in this paper are available online at http://ieeexplore.ieee.org.

Digital Object Identifier 10.1109/TPEL.2017.2747139

of MEE and output voltage regulation at steady state, it does not give good dynamic regulation of the output voltage during the MEE tracking process. Here, the series–series compensated WPT system is controlled by a discrete proportional-integral (PI) control scheme. It performs poorly in responding to fast dynamic changes of coupling coefficient, quality factor, and load conditions, of which the process of MEE tracking may induce large overshoot/undershoot and longer settling time of the output voltage. This may shorten the lifetime and even damage the load in which it is connected to.

To achieve a consistent and optimized dynamic performance of the series–series compensated WPT system in the event of unknown and wide-range changes, the replacement of the discrete PI control scheme with a discrete sliding mode control (DSMC) scheme is proposed in this paper. Sliding mode control (SMC) is naturally well suited for the control of power converters [30]. It consists of a time-varying state-feedback discontinuous control law that switches at a high frequency from one continuous structure to another according to the present position of the state variables in the state space. SMC offers superior dynamic performance for power converters in a wide operating range [31]. However, most of the SMC are implemented in analog controller forms [32]–[34]. Studies on DSMC for digital controllers are relatively limited [35]–[37], much less the applications [38], [39]. The applied DSMC for the WPT system is inherited from the equivalent SMC described in [32]. The implementation of the DSMC can be briefly described as a derived equivalent control signal based on the discrete SMC law to be modulated by the time-based counter of digital controllers. Compared to conventional discrete PI control, only one more current sensor for the output capacitor current is required.

In this paper, a hill-climbing-search-based phase angle control is used with the dc/ac converter to achieve minimum input current, thereby attaining minimum input power control. The algorithm of the phase angle control is designed by considering the working principle of digital controllers. The phase angle control renders the series–series compensated WPT system with MEE, but does not contribute to the dynamic improvement. Still, the dynamic improvement of the output voltage is still significant when the series–series compensated WPT system is controlled by the proposed DMSC scheme. This paper is an extension of the conference paper [40].

II. Difference Between MEE and MPT of the WPT System

A schematic diagram of the series–series compensated WPT system is depicted, as shown in Fig. 1, where $V_{\rm dc}$ is the dc power supply; L_1 and L_2 are the self-inductance of the primary and the secondary windings; R_{p1} and R_{p2} are the equivalent resistances of the primary and the secondary windings, respectively; M_{12} is the mutual inductance of the two windings; C_1 and C_2 denotes the compensating capacitors required for compensating the large leakage inductance and also for blocking the dc voltage offset caused by the inverting bridge; $C_{\rm b}$ is the filtering capacitance; L and C are the energy storage components of the buck–boost converter; and R is the resistance of load.

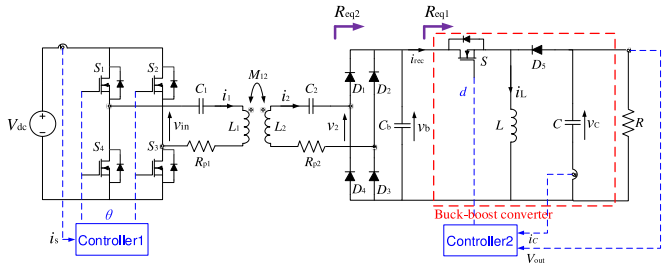

Fig. 1. Schematic diagram of the series–series compensated WPT system with noncommunication controllers.

In Fig. 1, the buck–boost converter (on the right-side of the figure) can operate in continuous conduction mode (CCM) or discontinuous conduction mode (DCM), depending upon the inductance value of L. If $L \geq \frac{D(1-D)V_{\rm dc}}{2i_L f_{s1}}$, where D is the duty ratio of switch S, i_L is the inductor current, and f_{s1} is the switching frequency, the buck–boost converter is operating in CCM with a load R, which has a corresponding equivalent impedance of

$$R_{\rm eq1CCM} = \frac{(1-D)^2}{D^2}R. \tag{1}$$

Conversely, if $L < \frac{D(1-D)V_{\rm dc}}{2i_L f_{s1}}$, the buck–boost converter operates in DCM with the load R with an equivalent impedance of

$$R_{\rm eq1DCM} = \frac{2Lf_{s1}}{D^2}. \tag{2}$$

By taking both (1) and (2) into consideration, the equivalent impedance can be generally expressed as follows:

$$R_{\rm eq1} = \frac{\left[(1-D)^2 R - 2Lf_{s1}\right]\kappa + 2Lf_{s1}}{D^2} \tag{3}$$

where $\kappa \epsilon \{0,1\}$ $\kappa = 1$ indicates that the buck–boost converter is operating in CCM and $\kappa = 0$ indicates that it is operating in DCM.

An equivalent impedance $R_{\rm eq2}$ can be further derived from (3) by incorporating the diode rectifier and the filtering capacitor $C_{\rm b}$. Based on the extended describing function [24], all the higher harmonics can be neglected as the resonant tank is tuned to fundamental harmonic as $v_2 = \frac{4}{\pi}v_b(\omega t)$, where $\omega = 2\pi f_s$ and f_s is the switching frequency of the dc/ac converter. Then, the root-mean-square (RMS) value of v_2 is $\frac{2\sqrt{2}}{\pi}v_b$. Similarly, the RMS value of i_2 can be derived as $\frac{\sqrt{2}\pi}{4}i_{\rm rec}$. Hence, the equivalent impedance $R_{\rm eq2}$ is

$$\begin{aligned} R_{\rm eq2} &= \frac{v_{2\rm rms}}{i_{2\rm rms}} = \frac{8}{\pi^2}R_{\rm eq1} \\ &= \frac{\left[8(1-D)^2 R - 16Lf_{s1}\right]\kappa + 16Lf_{s1}}{\pi^2 D^2} \end{aligned} \tag{4}$$

where $v_{2\rm rms}$ is the RMS value of v_2 and $i_{2\rm rms}$ is the RMS value of i_2.

A simplified schematic diagram of the series–series compensated WPT system expressed in terms of the equivalent impedance can be drawn, as shown in Fig. 2.

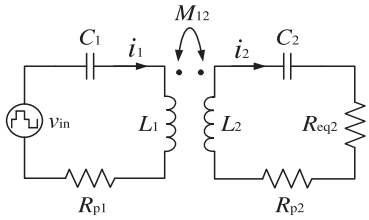

Fig. 2. Simplified schematic diagram of the series–series compensated WPT system.

Then, the energy efficiency of the system can be derived by neglecting the core loss of the magnetic ferrite plates as follows: (5) as shown at the bottom of this page.

The MEE of the WPT system can be achieved by controlling the duty ratio to satisfy

$$\frac{\partial \eta}{\partial D} = \frac{\partial \eta}{\partial R_{\mathrm{eq2}}} \frac{\partial R_{\mathrm{eq2}}}{\partial D} = 0 \tag{6}$$

and

$$D_{\mathrm{MEE}} = \frac{1}{\kappa + \frac{\sqrt{2}\pi}{4} \sqrt{\frac{R_{\mathrm{p2}}}{2Lf_{s1} + \kappa(R - 2Lf_{s1})}} \sqrt{1 + \frac{\omega^2 M_{12}^2}{R_{p1} + R_{\mathrm{p2}}}}}. \tag{7}$$

The output power of the system is

$$P_{\mathrm{out}} = \frac{V_{\mathrm{out}}^2}{R} = i_{2\mathrm{rms}}^2 R_{\mathrm{eq2}} = \frac{\omega^2 M_{12}^2 v_{\mathrm{in}}^2 R_{\mathrm{eq2}}}{\left(\omega^2 M_{12}^2 + R_{p1} R_{p2} + R_{p1} R_{\mathrm{eq2}}\right)^2 + \left(R_{p2} + R_{\mathrm{eq2}}\right)^2 \left(\omega L_1 - \frac{1}{\omega C_1}\right)^2}. \tag{8}$$

The MPP of the WPT system can be achieved by controlling the duty ratio to satisfy

$$\frac{\partial P_{\mathrm{out}}}{\partial D} = \frac{\partial P_{\mathrm{out}}}{\partial R_{\mathrm{eq2}}} \frac{\partial R_{\mathrm{eq2}}}{\partial D} = 0 \tag{9}$$

and

$$D_{\mathrm{MPT}} = \frac{1}{\kappa + \frac{\sqrt{2}\pi}{4} \sqrt{\frac{R_{\mathrm{p2}}}{2Lf_{s1} + \kappa(R - 2Lf_{s1})}} \left(1 + \frac{\omega^2 M_{12}^2}{R_{p1} + R_{\mathrm{p2}}}\right)}. \tag{10}$$

Apparently, $D_{\mathrm{MPT}} \neq D_{\mathrm{MEE}}$. The control objectives of the WPT system to track the MEE and MPT are different, which confirms the conclusions drawn in [29]. In this paper, the energy efficiency is the primary concern. Therefore, the WPT system is designed to operate under the MEE principle.

III. Minimum Input Power by Phase Angle Control

With any constant output load R, the output voltage V_{out} of the converter is generally regulated at the reference value such that the output power consumed by the load is fixed at the steady state. Therefore, MEE of the WPT system can be achieved by simply minimizing the input current i_s. For this purpose, a hill-climbing-search-based phase angle control is adopted to seek the minimum i_s. Specifically, the phase angle between the arm bridges of the dc/ac converter α is optimized via the phase angle control to regulate v_{in} based on the extended describing function

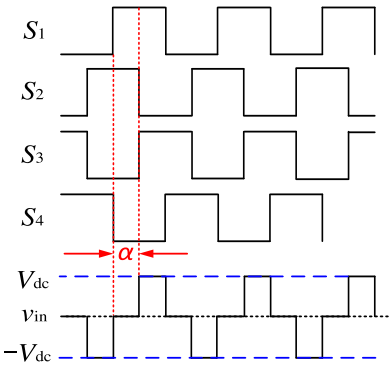

Fig. 3. Waveforms of the switching signals for the dc/ac converter and v_{in} (without the resonant tank).

$$v_{\mathrm{inrms}} = \frac{\sqrt{2} V_{\mathrm{dc}}}{\pi} g(\alpha) \tag{11}$$

where v_{inrms} is the RMS value of v_{in} and $g(\alpha) = \sqrt{\cos^2\alpha + \sin^2\alpha \cos^2\alpha + 2\cos\alpha + 1}$. Meanwhile, $i_{1\mathrm{rms}}$ (RMS value of i_1) can be derived as follows:

$$i_{1\mathrm{rms}} = \frac{R_{\mathrm{p2}} + R_{\mathrm{eq2}}}{R_{\mathrm{p1}} R_{\mathrm{p2}} + \omega^2 M_{12}^2} v_{\mathrm{inrms}}. \tag{12}$$

According to the energy conservation law and by neglecting the power loss of the dc/ac converter, we have

$$i_s = \frac{v_{\mathrm{inrms}} i_{1\mathrm{rms}}}{V_{\mathrm{dc}}} = \frac{2V_{\mathrm{dc}}^2 \left(R_{\mathrm{p2}} + R_{\mathrm{eq2}}\right)}{\pi^2 \left(R_{\mathrm{p1}} R_{\mathrm{p2}} + \omega^2 M_{12}^2\right)} g^2(\alpha). \tag{13}$$

Apparently, i_s can be regulated by the phase angle α. Fig. 3 depicts the waveforms of the switching signals and the corresponding waveform of v_{in} (without the resonant tank).

Fig. 4 depicts the flowchart of the hill-climbing-search-based phase angle control.

The process can be described as follows.

1) An initial phase angle $\alpha(0)$ is applied to the dc/ac converter and the input current $i_s(0)$ is measured.
2) The phase angle α is increased by an incremental angle $\Delta\alpha$ at the next sampling time and the input current $i_s(1)$ is measured.
3) The directions of the hill-climbing search (increase or decrease $\Delta\alpha$) can be determined by the comparison between $i_s(0)$ and $i_s(1)$. If $i_s(1) < i_s(0)$, which means the increase of α approaches the objective of finding the optimal phase angle α_{opt}, α is continuously increased by applying $\alpha(k+1) = \alpha(k) + \Delta\alpha$. Here, k indicates the sampling

$$\eta = \frac{i_{2\mathrm{rms}}^2 R_{\mathrm{eq2}}}{i_{1\mathrm{rms}}^2 R_{p1} + i_{2\mathrm{rms}}^2 \left(R_{\mathrm{eq2}} + R_{p2}\right)} = \frac{\omega^2 M_{12}^2 R_{\mathrm{eq2}}}{\left[\left(R_{\mathrm{eq2}} + R_{p2}\right)^2 + \left(\omega L_2 - \frac{1}{\omega C_2}\right)^2\right] R_{p1} + \omega^2 M_{12}^2 \left(R_{\mathrm{eq2}} + R_{p2}\right)}. \tag{5}$$

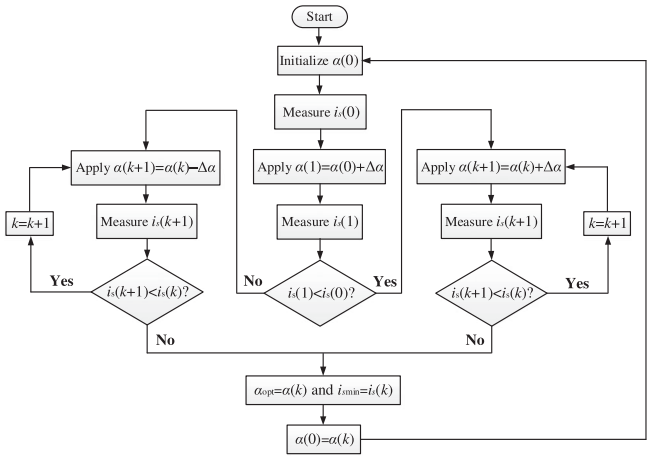

Fig. 4. Flowchart of the hill-climbing-search-based phase angle control.

time kT_s, where T_s is the sampling period of the phase angle control for the dc/ac converter. If $i_s(1) \geq i_s(0)$, which means the increase of α deviates from $\alpha_{\rm opt}$, α is to be decreased by applying $\alpha(k+1) = \alpha(k) - \Delta\alpha$.

4) For both directions of the hill-climbing search, the measured input current at the sampling time k+1 are compared to the input current at the previous sampling time k. If $i_s(k+1) < i_s(k)$, which means the tendency of increasing or decreasing α is correct, $\alpha(k+1) = \alpha(k) + \Delta\alpha$ or $\alpha(k+1) = \alpha(k) - \Delta\alpha$ should continuously be conducted to let α approach $\alpha_{\rm opt}$. If $i_s(k+1) \geq i_s(k)$, which means the change of α cannot further decrease the input current, $\alpha(k)$ can be considered as $\alpha_{\rm opt}$ and the corresponding $i_s(k)$ is the minimum input current.
5) $\alpha(k)$ is used as $\alpha(0)$ for the next iteration to ensure that the minimum input current $i_{\rm smin}$ can always be achieved even if the operating condition of the system is changed. When $\alpha_{\rm opt}$ and $i_{\rm smin}$ are found, the minimum input power of the WPT system can be reached. Meanwhile, if the output voltage of the load is regulated to meet the reference simultaneously, the MEE of the WPT system can be implemented.

IV. Output Voltage Regulation by DSMC

Conventionally, the PI control is the common approach for regulating the buck–boost converter of the receiver. Such a controller implemented in the discrete PI control form adopts a control equation

$$\Delta u(k) = K_p \Delta e(k) + K_i e(k) \tag{14}$$

where $\Delta u(k) = u(k) - u(k-1)$ is the increment of the control signal at the sampling time kT_{s1}. T_{s1} is the sampling period of the digital PI control; $e(k) = V_{\rm ref} - V_{\rm out}$ is the error between the reference and the control variable, where $V_{\rm ref}$ is the reference of the output voltage and $V_{\rm out}$ is the measured output voltage; $\Delta e(k) = e(k) - e(k-1)$ is the increment of the error; $K_{\rm p}$ is the proportional tuning coefficient, and $K_{\rm i}$ is the integral tuning coefficient of the discrete PI controller. Then,

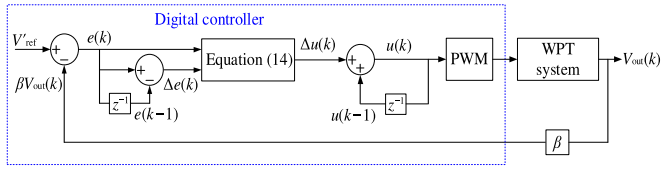

Fig. 5. Control block diagram of the discrete PI control for the WPT system.

the increment of control signal $\Delta u(k)$ is added to the control signal $u(k-1)$ at the previous sampling time to render the present control signal $u(k)$. The control block diagram of the discrete PI control for the WPT system is shown in Fig. 5. Here, β is the coefficient of the output voltage to enable analog-to-digital conversion (ADC) of the digital controller. Specifically, the measured voltage (around 10 V for this case) is out of the range of the ADC requirements (0–3.6 V for this case); $V'_{\rm ref} = \beta V_{\rm ref}$ is the scaled down reference; and PWM is short for pulse width modulation.

However, the use of PI control (since it is a form linear control) limits its effectiveness in giving good voltage regulation to small regions within a predesigned operating point of the WPT system. In the cases of the hill-climbing search process and load-point change, the phase angle will be periodically changed. The output voltage will suffer from high overshoot/undershoot and long settling time during the transient states if the WPT system is regulated by the discrete PI control. To overcome such a dynamic issue, a DSMC is therefore adopted to mitigate these undesired phenomena. The control variables $\mathbf{x}(k)$ are expressed in the following form:

$$\begin{aligned} \mathbf{x}(k) &= \begin{bmatrix} x_1(k) \\ x_2(k) \\ x_3(k) \end{bmatrix} \\ &= \begin{bmatrix} V'_{\rm ref} - \beta V_{\rm out}(k) \\ \frac{\beta}{T_{s1}} \left[V_{\rm out}(k) - V_{\rm out}(k+1) \right] \\ T_{s1} \sum_{j=0}^{k-1} \left[V'_{\rm ref} - \beta V_{\rm out}(j) \right] \end{bmatrix} \end{aligned} \tag{15}$$

where β is also defined as the coefficient to enable ADC of the digital controller. Then, the discrete state-space model required for the controller design can be derived as follows:

$$\begin{aligned} \mathbf{x}(k+1) &= \begin{bmatrix} x_1(k+1) \\ x_2(k+1) \\ x_3(k+1) \end{bmatrix} = \begin{bmatrix} 1 & T_{s1} & 0 \\ 0 & 1 - \frac{T_{s1}}{RC} & 0 \\ T_{s1} & 0 & 1 \end{bmatrix} \begin{bmatrix} x_1(k) \\ x_2(k) \\ x_3(k) \end{bmatrix} \\ &\quad + \begin{bmatrix} 0 \\ \frac{\beta T_{s1} V_{\rm out}(k)}{LC} - \frac{\beta T_{s1} V_{\rm out}(k)}{LC} u(k) \\ 0 \end{bmatrix}. \end{aligned} \tag{16}$$

The sliding surface of the DSMC is given as follows:

$$s(k) = \alpha_1 x_1(k) + \alpha_2 x_2(k) + \alpha_3 x_3(k) \tag{17}$$

where α_1, α_2, and α_3 are sliding coefficients. To ensure the stability of the sliding surface, $\alpha_1 > 0$, $\alpha_2 > 0$, and $\alpha_3 > 0$ are preliminary design conditions based on the Routh–Hurwitz

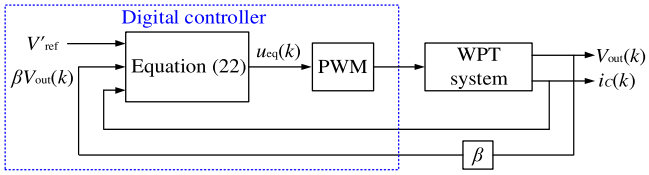

Fig. 6. Control block diagram of the DSMC for the WPT system.

criterion. Besides, the local reachability condition of the sliding mode operation must be satisfied [35]

$$[s(k+1) - s(k)]\,\mathrm{sgn}(s(k)) < 0 \tag{18}$$

where sgn(.) is the sign function.

If $s(k) \to 0^+$, $s(k+1) < s(k)$. Substituting $u(k) = 1$, (16), and (17) into (18) gives

$$0 < \left(\frac{\alpha_1\beta L}{\alpha_2} - \frac{\beta L}{RC}\right) i_C(k) - \frac{\alpha_3 LC}{\alpha_2}\left[V'_{\rm ref} - \beta V_{\rm out}(k)\right] \tag{19}$$

where i_C is the output capacitor current.

If $s(k) \to 0^-$, $s(k+1) > s(k)$. Substituting $u(k) = 0$, (16), and (17) into (18) gives

$$x\left(\frac{\alpha_1\beta L}{\alpha_2} - \frac{\beta L}{RC}\right) i_C(k) - \frac{\alpha_3 LC}{\alpha_2}\left[V'_{\rm ref} - \beta V_{\rm out}(k)\right] < \beta V_{\rm out}(k)\cdot \tag{20}$$

Finally, the combination of (19) and (20) gives the simplified existence condition

$$0 < \left(\frac{\alpha_1\beta L}{\alpha_2} - \frac{\beta L}{RC}\right) i_C(k) - \frac{\alpha_3 LC}{\alpha_2}\left[V'_{\rm ref} - \beta V_{\rm out}(k)\right] < \beta V_{\rm out}(k)\cdot \tag{21}$$

Then, the equivalent control signal $u_{\rm eq}(k)$ can be obtained by letting $s(k+1) = s(k)$ to give

$$u_{\rm eq}(k) = 1 - \frac{K_1}{V'_{\rm ref}} + \frac{K_1}{\beta V_{\rm out}(k)} + \frac{K_2 i_C(k)}{\beta V_{\rm out}(k)} \tag{22}$$

where $K_1 = \frac{\alpha_3 LCV'_{\rm ref}}{\alpha_2}$ and $K_2 = \frac{\beta L}{RC} - \frac{\alpha_1\beta L}{\alpha_2}$ are the tuning coefficients of the DSMC; $0 \le u_{\rm eq}(k) < 1$. $u_{\rm eq}(k)$ can be translated to the instantaneous duty ratio $d(k)$ of the PWM [30], which is more suitable for digital controllers. Computational delays (accounting for the time duration of sampling, ADC conversion, PWM reference calculation, and updating) and PWM delays (zero-order-hold effect) are approximately 1.5 times sampling periods (T_s and T_{s1}). They are negligible because the sampling frequency of the digital controllers used in this paper is much faster than the switching frequency for the power converters. The control block diagram of the DSMC for the WPT system is shown in Fig. 6.

V. Simulation Results

Simulation studies are conducted using the software platforms PSIM10 and MATLAB/SIMULINK to compare the performance of the discrete PI control and the DSMC for the WPT system under the MEE principle. The circuit part is implemented in PSIM10 and the control part including the phase angle control, the discrete PI control, and the DSMC scheme, is implemented in MATLAB/SIMULINK. A SimCoupler module is used to link up the two software platforms. The sampling frequency for both PSIM10 and MATLAB are set at 14 MHz. The specifications of the main circuit components are listed in Table I. The parameters of the phase angle control, the discrete PI control, and the DSMC are provided in Table II. In simulation, β can be implemented as a control block. The switching frequency f_{s1} is the same for both the discrete PI control and the DSMC.

TABLE I
Specifications of Main Components in the WPT System

Parameter	Value	Parameter	Value
$V_{\rm dc}$	10 V	C_1	27.76 nF
C_2	27.6 nF	R_{p1}	0.441 Ω
R_{p2}	0.415 Ω	L_1	91.24 μH
L_2	91.77 μH	M_{12}	6.3 μH
$C_{\rm b}$	2 μF	L	50 μH
C	100 μF	R	18 Ω

TABLE II
Parameters of the Controllers

Parameter	Value	Parameter	Value
$V_{\rm ref}$	10 V	β	0.25
$K_{\rm p}$	0.4	$K_{\rm i}$	200
K_1	20	K_2	−0.8
f_s	100 kHz	f_{s1}	20 kHz

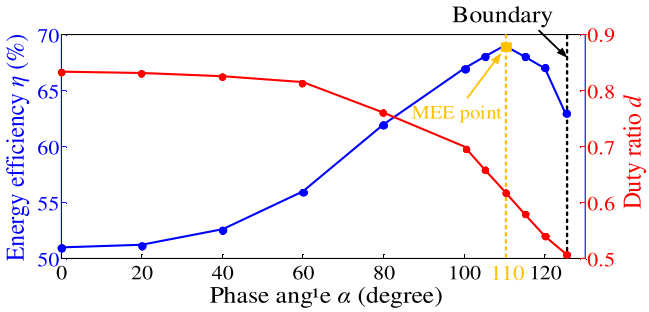

Fig. 7. Relationship between η, d, and α when the WPT system is controlled by the phase angle control and the DSMC.

Fig. 7 shows the results of the relationship between the phase angle α, duty ratio of the buck–boost converter d, and the energy efficiency η, when the WPT system is controlled by the phase angle control and the DSMC. As mentioned in [28], the MEE point will only appear at the side of the boundary where the output power decreases with the increase of d. Therefore, only the side with MEE point is investigated. The boundary of the phase angle is 125° and the MEE point is at 110° with a duty ratio of 0.62 and energy efficiency of 69%. The MEE of 69% highly depends on the mutual inductance and the resistance of the load in the WPT system. When the mutual inductance increases (distance between coils reduces), the MEE will increase and

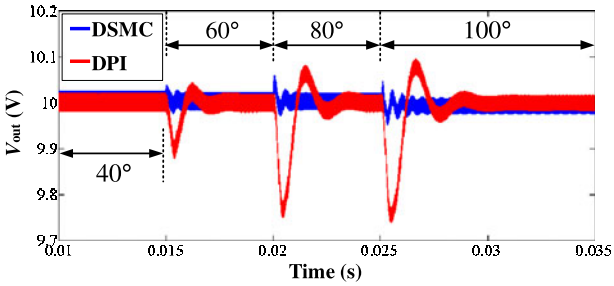

Fig. 8. Comparisons of $V_{\rm out}$ between the discrete PI control and the DSMC for the WPT system.

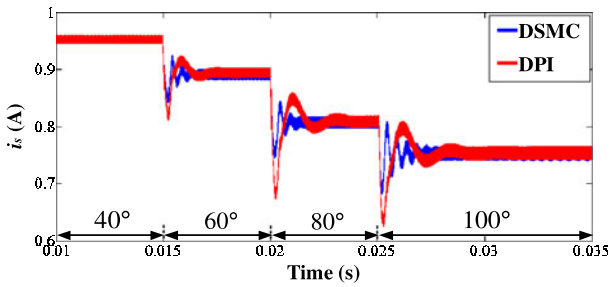

Fig. 9. Comparisons of i_s between the discrete PI control and the DSMC for the WPT system.

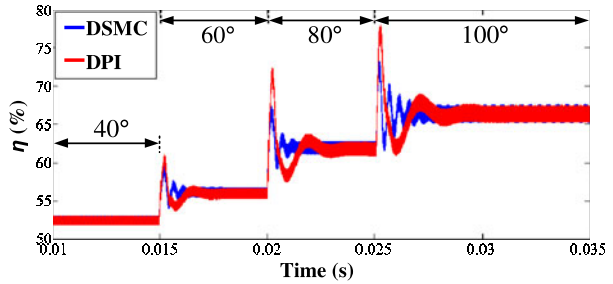

Fig. 10. Comparisons of η between the discrete PI control and the DSMC for the WPT system.

vice versa. When the resistance of the load increases, the MEE will decrease and vice versa. Besides, the voltage drops of the diodes in the diode rectifier and the buck–boost converter will distinctly affect the MEE of the WPT system. The steady-state performance of the WPT system controlled by the phase angle control and the DSMC is well verified by matching the results with that of the conventional control scheme.

Then, the comparisons of the output voltage $V_{\rm out}$, the input current i_s, and the instantaneous energy efficiency η between the DSMC and the discrete PI control during transient states are given in Figs. (8)–(10), respectively. The discrete PI controller is designed for the operating condition of 0° phase angle, such that the parameters of the discrete PI controller are optimally designed for that operating point. Apparently, the dynamic performance of the output voltage $V_{\rm out}$, the input current i_s, and the instantaneous energy efficiency η are distinctly improved by the DSMC with less overshoot and shorter settling time when the phase angle α is regulated from 40° to 100° with $\Delta\alpha = 20°$ and the period of 5 ms.

TABLE III
PARAMETERS OF THE PRACTICAL RESONATORS

Parameter	Value	Parameter	Value
Coil diameter	31 cm	Wire diameter	1.2 mm
Number of turns	11	Length of the winding	15 mm

VI. EXPERIMENTAL VERIFICATION

The experiment is conducted on a two-coil series–series compensated WPT system with the parameters given in Table I. The parameters of the practical resonators are provided in Table III, where the length of the winding indicates the length from the first turn to the eleventh turn. The controllers used for both the dc/ac converter of the transmitter and the buck–boost converter of the receiver are low-cost microcontroller unit (MCU) STM32VLDISCOVERY with a sampling frequency of 14 MHz. Full schematic diagram of the WPT system in the experiment is shown in Fig. 11. The codes of the phase angle control based on the algorithm given in Fig. 4 are programmed in the MCU of control stage 1. The codes of the DSMC based on (22) and the discrete PI control based on (14) are programmed in the MCU of control stage 2. A photograph of the experiment setup is shown in Fig. 12.

The experiment is initially carried out with the WPT system controlled by the phase angle control and the DSMC to examine the steady-state performance. Fig. 13 shows the searching process of the input current $i_{\rm s}$ in reaching the MEE point of the WPT system. $i_{\rm s}$ finally reaches the minimum input current at about 0.95 A through the regulation of the phase angle control. Besides, the energy efficiency η of the WPT system is calculated and compared. Fig. 14 shows a comparison of the energy efficiency η around the MEE point (the phase angle α, which ranges from 80° to 125° in steps of 5°) between the simulation and the experiment results. As shown, the MEE of the WPT system in practice is about 60%. This is attributed to the diverse energy loss in the hardware (additional voltage drops of diodes, resistance of cables and printed circuit board (PCB) routes, parasitic resistance of energy storage components, and energy loss in integrated circuits (ICs)), which are not modeled in the simulation. By applying the conventional control scheme described in [28], the MEE of the WPT system is almost equivalent to 60% as well.

Then, the comparison of the dynamic performance between the DSMC and the discrete PI control on the MEE tracking process is conducted. The discrete PI controller is designed to operate at 0° phase angle. Figs. (15)–(18) show the waveforms of the output voltage $V_{\rm out}$ and the corresponding switching signals during both transient and steady states when the buck–boost converter is regulated by the discrete PI control and the DSMC, respectively. In Fig. 15, the overshoot of the output voltage $V_{\rm out}$ during the transient state is about 2.5 V and the settling time is about 151.8 ms when the buck–boost converter is controlled by the discrete PI control when the phase angle α of the dc/ac

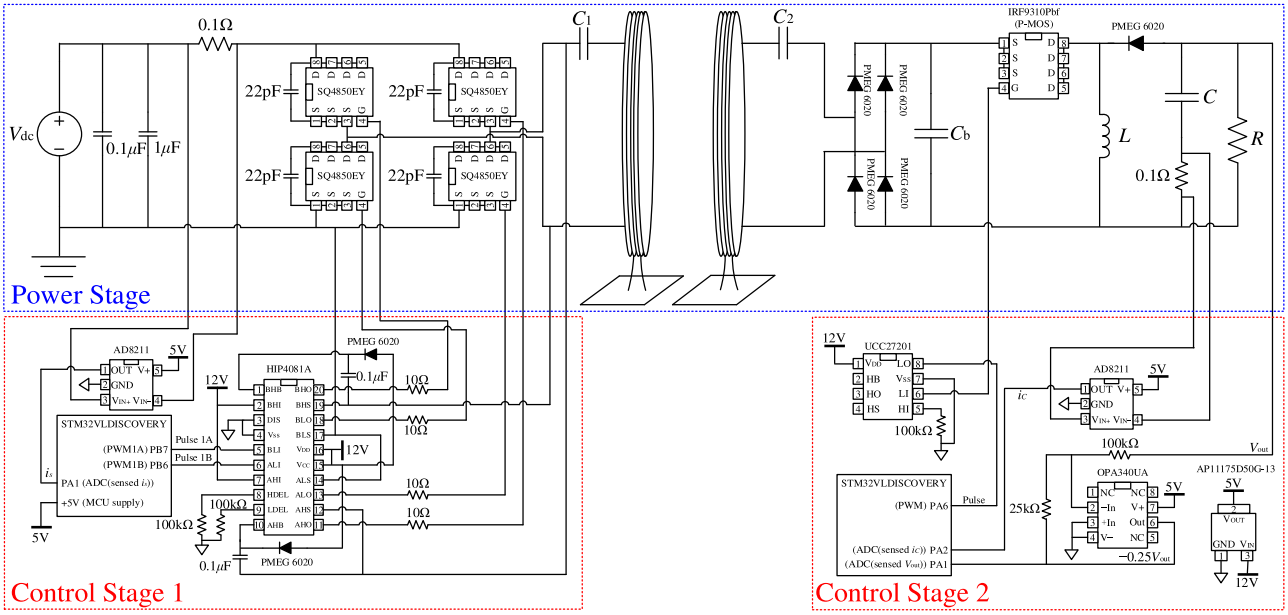

Fig. 11. Full schematic diagram of the WPT system in the experiment.

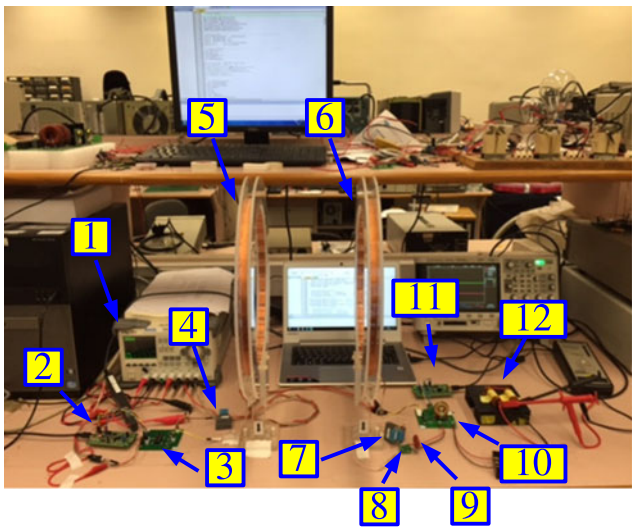

Fig. 12. Photograph of the experiment setup. [1: Power supply for $V_{\rm dc}$ and control stages; 2: STM32DISCOVERY for control stage 1; 3: dc/ac converter; 4: compensated capacitor C_1; 5: primary winding L_1; 6: secondary winding L_2; 7: compensated capacitor C_2; 8: diode rectifier; 9: filtering capacitor $C_{\rm b}$; 10: buck–boost converter; 11: STM32DISCOVERY for control stage 2; and 12: load R].

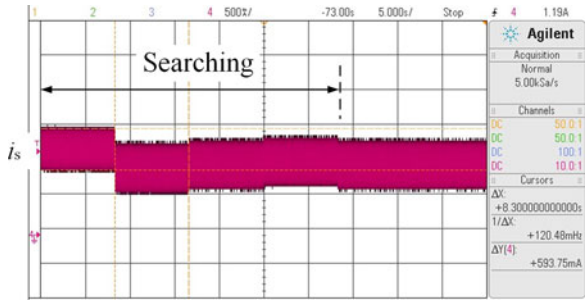

Fig. 13. Search process of the input current i_s to reach the MEE point.

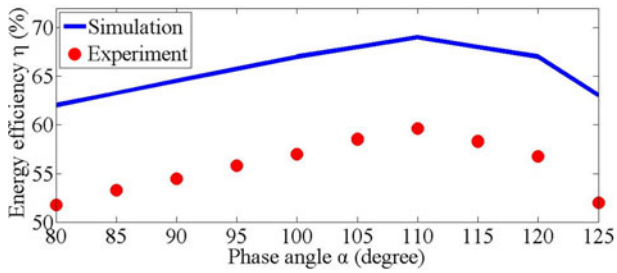

Fig. 14. Comparisons of the energy efficiency η between the simulation and the experiment results.

converter is changed from 120° to 100°. However, as shown in Fig. 16, the overshoot of the output voltage $V_{\rm out}$ during the transient state is about 2 V (80% of that with the discrete PI control) and the settling time is about 48 ms (31.6% of that with the discrete PI control) when the buck–boost converter is controlled by the DSMC with the phase angle α being changed from 120° to 100°.

In Fig. 17, the undershoot of the output voltage $V_{\rm out}$ during the transient state is about 2.0 V and the settling time is about 164.3 ms when the buck–boost converter is controlled by the discrete PI control when the phase angle α is changed from 100° to 110°. However, in Fig. 18, the undershoot of the output voltage $V_{\rm out}$ during the transient state is about 1.9 V and the settling time is about 39.3 ms (23.9% of that with the discrete PI control) when the buck–boost converter is controlled by the DSMC with the phase angle α being changed from 100° to 110°.

Similar comparisons between the discrete PI control and the DSMC are carried out when the phase angle α varies around

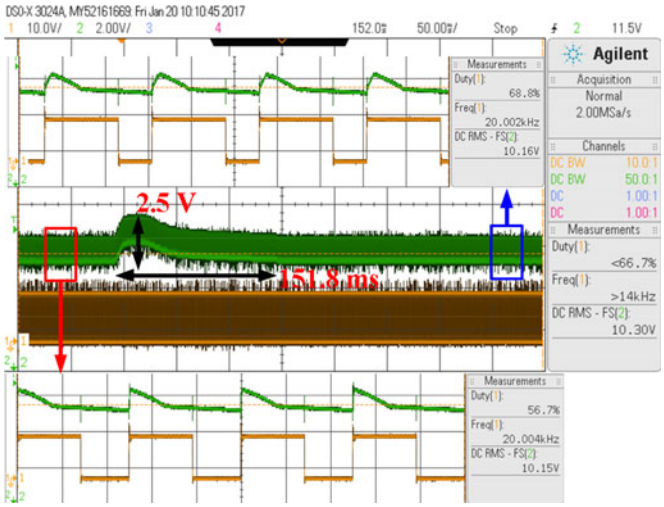

Fig. 15. Waveforms of $V_{\rm out}$ and the corresponding switching signals when the phase angle α is changed from 120° to 100° with the discrete PI control.

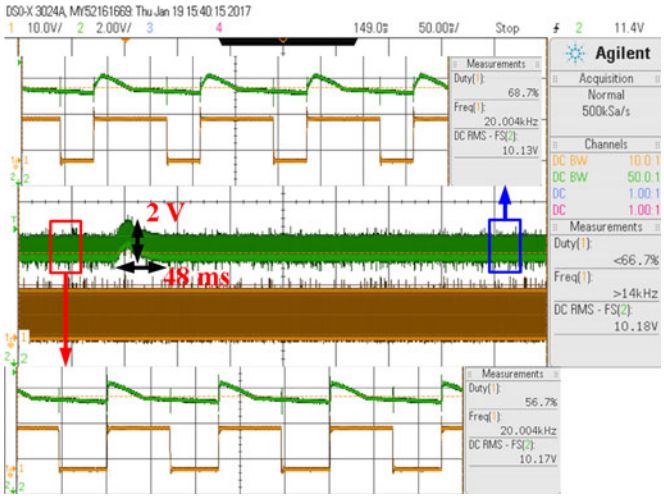

Fig. 16. Waveforms of $V_{\rm out}$ and the corresponding switching signals when the phase angle α is changed from 120° to 100° with the DSMC.

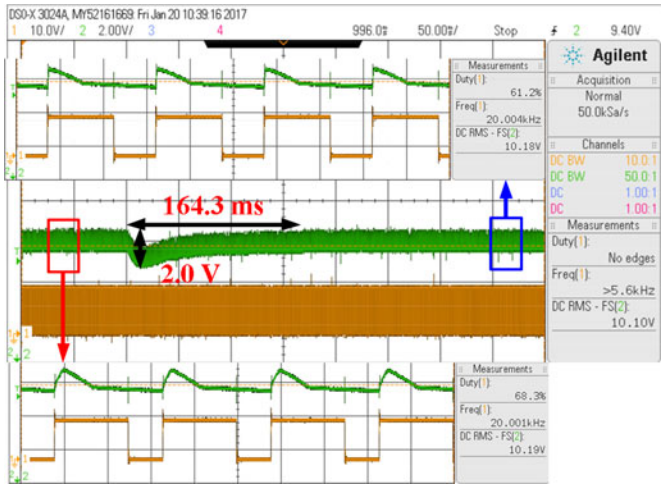

Fig. 17. Waveforms of $V_{\rm out}$ and the corresponding switching signals when the phase angle α is changed from 100° to 110° with the discrete PI control.

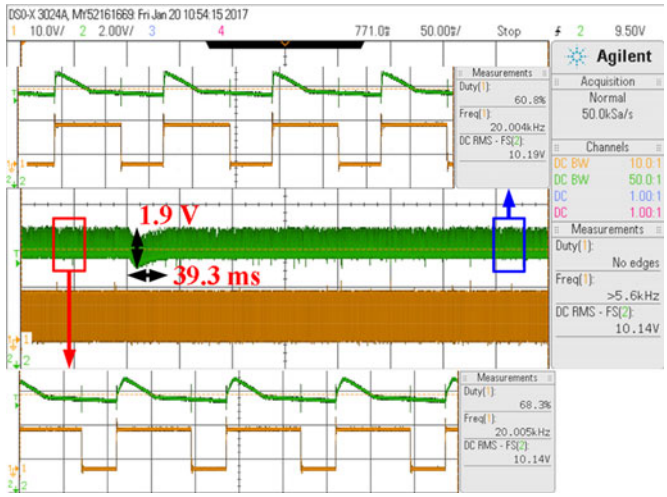

Fig. 18. Waveforms of $V_{\rm out}$ and the corresponding switching signals when the phase angle α is changed from 100° to 110° with the DSMC.

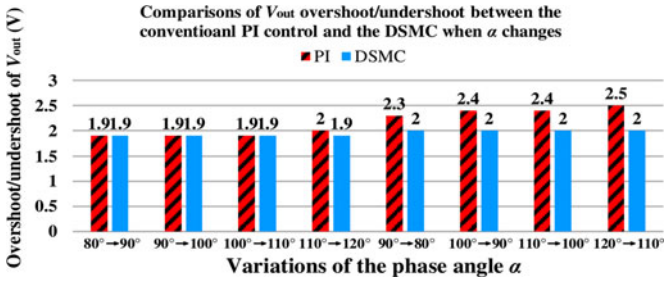

Fig. 19. Comparisons of the overshoot/undershoot of $V_{\rm out}$ between the discrete PI control and the DSMC when α varies around the MEE point.

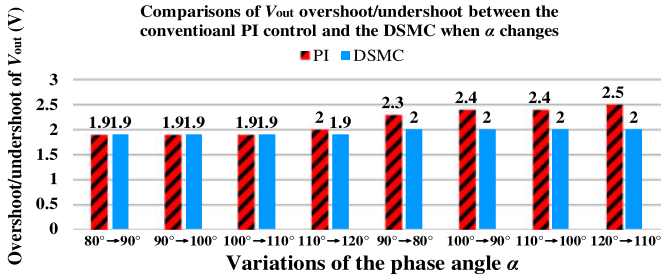

Fig. 20. Comparisons of the setting time of $V_{\rm out}$ between the discrete PI control and the DSMC when α varies around the MEE point.

the MEE point (80° to 120°) by $\Delta\alpha = 10°$. Comparisons of the overshoot/undershoot of the output voltage $V_{\rm out}$ during transient states are shown in Fig. 19 using histogram. As shown, the mitigation of the voltage undershoot (with an increasing α) is small with the DSMC scheme. However, the voltage overshoot reduction (with a decreasing α) achievable with the DSMC scheme is significant. The improvement is on average about 16.6%. Comparisons of the settling time of the output voltage $V_{\rm out}$ during transient states are shown in Fig. 20. The settling time is shortened significantly by using the DSMC. The improvement is on average about 72.9%.

VII. Conclusion

In this paper, a DSMC along with a phase angle control is applied to a two-coil series–series compensated WPT system under the MEE principle. Both simulation and experiment results validate that the dynamic performance of the output voltage of the WPT system during the MEE tracking are improved with the use of the proposed control scheme, as compared that of the conventional discrete PI control scheme. Experiment results show that the overshoot reduction is about 16.6% and the settling time is shortened by about 72.9% when the phase angle varies around the MEE point in steps of 10°. Such an improvement in the dynamic behavior of the WPT system is important for protecting the load in which it is connected to, from a possible high voltage overshoot during a long transient.

Acknowledgment

The authors would like to thank Prof. D. Hill.

References

[1] N. Tesla, "Apparatus for transmitting electrical energy," U.S. Patent 1 119 732, Dec. 1, 1914.

[2] W. H. Ko, S. P. Liang, and C. D. F. Fung, "Design of rf-powered coils for implant instruments," *Med. Biol. Eng. Comput.*, vol. 15, pp. 634–640, 1977.

[3] J. G. Bum and B. H. Cho, "An energy transmission system for an artificial heart using leakage inductance compensation of transcutaneous transformer," *IEEE Trans. Power Electron.*, vol. 13, no. 6, pp. 1013–1022, Nov. 1998.

[4] D. Ahn and S. Hong, "Wireless power transmission with self-regulated output voltage for biomedical implant," *IEEE Trans. Ind. Electron.*, vol. 61, no. 5, pp. 2225–2235, May 2014.

[5] W. G. Hurley and J. Kassakian, "Induction heating of circular ferromagnetic plates," *IEEE Trans. Magn.*, vol. MAG-15, no. 4, pp. 1174–1181, Jul. 1979.

[6] G. A. Covic, J. T. Boys, M. L. G. Kissin, and H. G. Lu, "A three-phase inductive power transfer system for roadway-powered vehicles," *IEEE Trans. Ind. Electron.*, vol. 54, no. 6, pp. 3370–3378, Dec. 2007.

[7] J. Huh, S. W. Lee, W. Y. Lee, G. H. Cho, and C. T. Rim, "Narrow-width inductive power transfer system for online electrical vehicles," *IEEE Trans. Power Electron.*, vol. 26, no. 12, pp. 3666–3679, Dec. 2011.

[8] J. Sallán, J. L. Villa, A. Llombart, and J. F. Sanz, "Optimal design of ICPT systems applied to electric vehicle battery charge," *IEEE Trans. Ind. Electron.*, vol. 56, no. 6, pp. 2140–2149, Jun. 2009.

[9] B. Choi, J. Nho, H. Cha, T. Ahn, and S. Choi, "Design and implementation of low-profile contactless battery charger using planar printed circuit board windings as energy transfer device," *IEEE Trans. Ind. Electron.*, vol. 51, no. 1, pp. 140–147, Feb. 2004.

[10] Y. Jang and M. M. Jovanovic, "A contactless electrical energy transmission system for portable-telephone battery chargers," *IEEE Trans. Ind. Electron.*, vol. 50, no. 3, pp. 520–527, Jun. 2003.

[11] C.-G. Kim, D.-H.Seo, J.-S. You, J.-H. Park, and B. H. Cho, "Design of a contactless battery charger for cellular phone," *IEEE Trans. Ind. Electron.*, vol. 48, no. 6, pp. 1238–1247, Dec. 2001.

[12] S. Y. R. Hui and W. C. Ho, "A new generation of universal contactless battery charging platform for portable consumer electronic equipment," *IEEE Trans. Power Electron.*, vol. 20, no. 3, pp. 620–627, May 2005.

[13] X. Liu and S. Y. R. Hui, "Simulation study and experimental verification of a contactless battery charging platform with localized charging features," *IEEE Trans. Power Electron.*, vol. 22, no. 6, pp. 2202–2210, Nov. 2007.

[14] S. Y. R. Hui, "Planar inductive battery charging system," U.S. Patent 7 576 514, Aug. 18, 2009.

[15] Wireless Power Consortium, *Qi System Description: Wireless Power Transfer, Volume I: Low Power, Part 1: Interface Definition, Version 1.1*. Piscataway, NJ, USA: Wireless Power Consortium, Apr. 2012.

[16] Wireless Power Consortium, 2016. [Online]. Available: http://www.wirelesspowerconsortium.com

[17] M. Budhia, G. A. Covic, J. T. Boys, and C.-Y. Huang, "Development and evaluation of single sided flux couplers for contactless electric vehicle charging," in *Proc. IEEE Energy Convers. Congr. Expo.*, Sep. 2011, pp. 614–621.

[18] S. Y. Choi, S. Y. Jeong, E. S. Lee, B. W. Gu, S. W. Lee, and C. T. Rim, "Generalized models on self-decoupled dual pick-up coils for large lateral tolerance," *IEEE Trans. Power Electron.*, vol. 30, no. 11, pp. 6434–6445, Feb. 2015.

[19] J. P. W. Chow, N. Chen, H. S. H. Chung, and L. L. H. Chan, "An investigation into the use of orthogonal winding in loosely coupled link for improving power transfer efficiency under coil misalignment," *IEEE Trans. Power Electron.*, vol. 30, no. 10, pp. 5632–5649, Nov. 2014.

[20] J. Deng, W. Li, T. D. Nguyen, S. Li, and C. C. Mi, "Compact and efficient bipolar coupler for wireless power chargers: Design and analysis," *IEEE Trans. Power Electron.*, vol. 30, no. 11, pp. 6130–6140, Mar. 2015.

[21] W. Zhang, S. C. Wong, C. K. Tse, and Q. Chen, "Design for efficiency optimization and voltage controllability of series-series compensated inductive power transfer systems," *IEEE Trans. Power Electron.*, vol. 29, no. 1, pp. 191–200, Jan. 2014.

[22] W. Li, H. Zhao, S. Li, J. Deng, T. Kan, and C. C. Mi, "Integrated LCC Compensation topology for wireless charger in electric and plug-in electric vehicles," *IEEE Trans. Ind. Electron.*, vol. 62, no. 7, pp. 4215–4225, Dec. 2014.

[23] A. K. Swain, M. J. Neath, U. K. Madawala, and D. Thrimawithana, "A dynamic multivariable state-space model for bidirectional inductive power transfer ssytems," *IEEE Trans. Power Electron.*, vol. 27, no. 11, pp. 4772–4780, Nov. 2012.

[24] Z. U. Zahid *et. al.*, "Modeling and control of series-series compensated inductive power transfer system," *IEEE J. Emerg. Sel. Top. Power Electron.*, vol. 3, no. 1, pp. 111–123, Mar. 2015.

[25] K. Aditya and S. S. Williamson, "Advanced controller design for a series-series compensated inductive power transfer charging infrastructure using asymmetrical clamped mode control," in *Proc. IEEE Appl. Power Electron. Conf. Expo.*, 2015, pp. 2718–2724.

[26] H. Takanashi, Y. Sato, Y. Kaneko, S. Abe, and T. Yasuda, "A large air gap 3 kW wireless power transfer system for electric vehicles," in *Proc. IEEE Energy Convers. Congr. Expo.*, 2012, pp. 269–274.

[27] C. K. Lee, W. X. Zhong, and S. Y. R. Hui, "Effects of magnetic coupling of non-adjacent resonators on wireless power domino-resonator systems," *IEEE Trans. Power Electron.*, vol. 27, no. 4, pp. 1905–1916, Apr. 2012.

[28] W. X. Zhong and S. Y. R. Hui, "Maximum energy efficiency tracking for wireless power transfer systems," *IEEE Trans. Power Electron.*, vol. 30, no. 7, pp. 4025–4034, Feb. 2015.

[29] S. Y. R. Hui, W. X. Zhong, and C. K. Lee, "A critical review of recent progress in mid-range wireless power transfer," *IEEE Trans. Power Electron.*, vol. 29, no. 9, pp. 4500–4511, Sep. 2014.

[30] R. Venkataramanan, A. Šabanović, and S. Ćuk, "Sliding mode control of DC-to-DC converters," in *Proc. IEEE Conf. Ind. Electron. Control Instrum.*, 1985, pp. 251–258.

[31] H. Sira-Ramirez and M. Ilic, "A geometric approach to the feedback control of switch mode DC-to-DC power supplies," *IEEE Trans. Circuits Syst.*, vol. 35, no. 10, pp. 1291–1298, Oct. 1988.

[32] S. C. Tan, Y. M. Lai, and C. K. Tse, *Sliding Mode Control of Switching Power Converters—Techniques and Implementation*. Boca Raton, FL, USA: CRC Press, 2012.

[33] R. J. Wai and L. C. Shih, "Design of voltage tracking control for DC-DC boost converter via total sliding-mode technique," *IEEE Trans. Ind. Electron.*, vol. 58, no. 6, pp. 2502–2511, Aug. 2010.

[34] Y. He and F. Luo, "Sliding-mode control for DC-DC converters with constant switching frequency," *IEE Proc. Control Theory Appl.*, vol. 153, no. 1, pp. 37–45, Jan. 2006.

[35] S. Z. Sarpturk, Y. Istefanopulos, and O. Kaynak, "On the stability of discrete-time sliding mode control system," *IEEE Trans. Automat. Control*, vol. TAC-32, no. 10, pp. 930–932, Oct. 1987.

[36] W. B. Gao, Y. F. Wang, and A. Homaifa, "Discrete-time variable structure control systems," *IEEE Trans. Ind. Electron.*, vol. 42, no. 2, pp. 117–122, Apr. 1995.

[37] X. Yu and G. Chen, "Discretization behaviors of equivalent control based sliding-mode control systems," *IEEE Trans. Automat. Control*, vol. 48, no. 9, pp. 1641–1646, Sep. 2003.

[38] S.-L. Jung and Y.-Y. Tzou, "Discrete sliding-mode control of a PWM inverter for sinusoidal output waveform synthesis with optimal sliding curve," *IEEE Trans. Power Electron.*, vol. 11, no. 4, pp. 567–577, Jul. 1996.

[39] T.-L. Tai and J.-S. Chen, "UPS inverter design using discrete-time sliding-mode control scheme," *IEEE Trans. Ind. Electron.*, vol. 49, no. 1, pp. 67–75, Aug. 2002.

[40] Y. Yang, W. X. Zhong, S. C. Tan, and S. Y. R. Hui, "Dynamic improvement of wireless power transfer systems with maximum energy efficiency tracking by sliding mode control," in *Proc. IEEE Int. Future Energy Electron. Conf., IEEE Energy Convers. Congr. Expo.*, Jun. 2017, pp. 1736–1740.

Yun Yang (S'13) received the B.S. degree in electrical engineering from Wuhan University, Wuhan, China, in 2012, and is currently working toward the Ph.D. degree in power electronics and control in Power Electronics Research Group, Department of Electrical and Electronic Engineering, The University of Hong Kong, Hong Kong.

His current research interests include modeling and control of power converters in smart grids, LED lighting systems, and wireless power transfer systems.

Wenxing Zhong (M'13) received the B.Eng. degree in electrical engineering from Tsinghua University, Beijing, China, in 2007, and the Ph.D. degree in wireless power transfer and power electronics from the City University of Hong Kong, Hong Kong, in 2012.

He is currently a Professor in the Department of Electrical Engineering, Zhejiang University, Hangzhou, China. From March 2016 to May 2017, he was a Research Assistant Professor in the Department of Electrical and Electronic Engineering, The University of Hong Kong. His current research interests include wireless power transfer and power electronics.

Mr. Zhong has received two Transactions First Prize Paper Awards from the IEEE Power Electronics Society since 2015.

Sitthisak Kiratipongvoot received the B.Eng. and M.Eng. degrees in electrical engineering from King Mongkut's University of Technology North Bangkok, Bangkok, Thailand, in 2001 and 2008, respectively.

From October 2008 to July 2012, he worked as a Research Assistant in the Department of Electronic and Information Engineering, Hong Kong Polytechnic University, Hong Kong. Since August 2012, he has been a Research Assistant in the Department of Electrical and Electronic Engineering, The University of Hong Kong, Hong Kong. His research interests include dc–dc converters, power factor correction ac–dc converters, resonant inverters, soft-switching techniques, renewable energy systems, electric vehicle, and wireless energy transfer.

Siew-Chong Tan (M'06–SM'11) received the B.Eng. (Hons.) and M.Eng. degrees in electrical and computer engineering from the National University of Singapore, Singapore, in 2000 and 2002, respectively, and the Ph.D. degree in electronic and information engineering from the Hong Kong Polytechnic University, Hong Kong, in 2005.

From October 2005 to May 2012, he worked as a Research Associate, Postdoctoral Fellow, Lecturer, and Assistant Professor in the Department of Electronic and Information Engineering, Hong Kong Polytechnic University. From January to October 2011, he was a Senior Scientist in the Agency for Science, Technology and Research, Singapore. He is currently an Associate Professor in the Department of Electrical and Electronic Engineering, The University of Hong Kong, Hong Kong. From September to October 2009, he was a Visiting Scholar at Grainger Center for Electric Machinery and Electromechanics, University of Illinois at Urbana–Champaign, Champaign, IL, USA, and an Invited Academic Visitor of Huazhong University of Science and Technology, Wuhan, China, in December 2011. His research interests are focused in the areas of power electronics and control, LED lightings, smart grids, and clean energy technologies. He is a coauthor of the book *Sliding Mode Control of Switching Power Converters: Techniques and Implementation* (CRC Press, 2011).

Dr. Tan serves extensively as a Reviewer for various IEEE/IET transactions and journals on power, electronics, circuits, and control engineering. He is an Associate Editor of the IEEE TRANSACTIONS ON POWER ELECTRONICS.

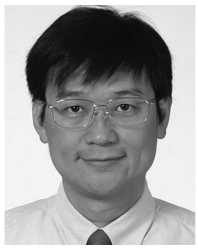

Shu Yuen Ron Hui (M'87–SM'94–F'03) received the B.Sc. (Eng) (Hons.) degree in electrical and electronic engineering from the University of Birmingham, Birmingham, U.K., in 1984, and the D.I.C. and Ph.D. degrees in electrical engineering from Imperial College London, London, U.K., in 1987.

He currently holds the Philip Wong Wilson Wong Chair Professorship at the University of Hong Kong, Hong Kong, and a part-time Chair Professorship at Imperial College London. He has published more than 300 technical papers, including more than 220 refereed journal publications. More than 60 of his patents have been adopted by industry. His inventions on wireless charging platform technology underpin key dimensions of Qi, the world's first wireless power standard, with freedom of positioning and localized charging features for wireless charging of consumer electronics.

Prof. Hui is an Associate Editor of the IEEE TRANSACTIONS ON POWER ELECTRONICS and the IEEE TRANSACTIONS ON INDUSTRIAL ELECTRONICS, and an Editor of the IEEE JOURNAL OF EMERGING AND SELECTED TOPICS IN POWER ELECTRONICS. He received the IEEE Rudolf Chope R&D Award from the IEEE Industrial Electronics Society, the IET Achievement Medal (The Crompton Medal) in 2010, and the IEEE William E. Newell Power Electronics Award in 2015. He is a Fellow of the Australian Academy of Technological Sciences and Engineering and the Royal Academy of Engineering, U.K.